# Group-common and individual-specific effects of structure-function coupling in human brain networks with graph neural networks

Peiyu Chen[1,#], Hang Yang[1,#], Xin Zheng[1], Hai Jia[1], Jiachang Hao[1], Xiaoyu Xu[1,2], Chao Li[3], Xiaosong He[4], Runsen Chen[5], Tatsuo S. Okubo[1,*], Zaixu Cui[1,*]

[1]Chinese Institute for Brain Research, Beijing, 102206, China

[2]State Key Laboratory of Cognitive Neuroscience and Learning, Beijing Normal University, Beijing, 100091, China

[3]Department of Applied Mathematics and Theoretical Physics, Department of Clinical Neurosciences, University of Cambridge, Cambridge, CB3 0WA, UK

[4]Department of Psychology, School of Humanities and Social Sciences, University of Science and Technology of China, Hefei, Anhui, 230026, China

[5]Vanke School of Public Health, Tsinghua University, Beijing, China

[#]Co-first author

[*]Correspondence: cuizaixu@cibr.ac.cn (Z.C.); tatsuo.okubo@cibr.ac.cn (T.S.O.)

**Abstract**

The human cerebral cortex is organized into functionally segregated but synchronized regions bridged by the structural connectivity of white matter pathways. While structure-function coupling has been implicated in cognitive development and neuropsychiatric disorders, studies yield inconsistent findings. The extent to which the structure-function coupling reflects reliable individual differences or primarily group-common characteristics remains unclear, at both the global and regional brain levels. By leveraging two independent, high-quality datasets, we found that the graph neural network accurately predicted unseen individuals' functional connectivity from structural connectivity, reflecting a strong structure-function coupling. This coupling was primarily driven by network topology and was substantially stronger than that of the linear models. Moreover, we observed that structure-function coupling was dominated by group-common effects, with subtle yet significant individual-specific effects. The regional group and individual effects of coupling were hierarchically organized across the cortex along a sensorimotor-association axis, with lower group and higher individual effects in association cortices. These findings emphasize the importance of considering both group and individual effects in understanding cortical structure-function coupling, suggesting insights into interpreting individual differences of the coupling and informing connectivity-guided therapeutics.

## Introduction

The human cerebral cortex is organized into functionally segregated neuronal populations connected by anatomical pathways. White matter fiber tracts form a connectome of structural connectivity at the macroscale[1]. This structural connectome exhibits a complex network topology characterized by non-random properties, including small-world architecture[2], segregated communities[3], and a core of densely interconnected hubs[4]. These topological patterns support the communication dynamics of structural networks and coordinate the temporal synchronization of neural activity, termed functional connectivity, between cortical regions[5-8]. Understanding how structural connectivity shapes functional connectivity patterns is central to neuroscientific research.

Convergent evidence from multiple independent studies suggests a reliable coupling between structural and functional connectivity at both global and regional brain levels, using non-invasive magnetic resonance imaging (MRI) techniques and invasive recordings[9-23]. The structure-function coupling is heterogeneously distributed across the cerebral cortex, exhibiting higher coupling in the primary sensorimotor cortex and lower coupling in the higher-order association cortex[10-12]. This spatial distribution pattern aligns with the sensorimotor-association cortical hierarchy of cytoarchitectonic structure, functional specialization, and evolutionary expansion[10,11,24]. The structure-function coupling shows a developmental increase at regions of association cortex during the adolescence with the most prominent effects localized in the default mode network[10]. In contrast, the highly evolutionarily conserved sensorimotor regions exhibit age-related decreases in structure-function coupling throughout adolescence[10] and the whole lifespan[13]. Moreover, higher structure-function coupling has been related to better performance in executive function[10,22], and the abnormal pattern of the coupling is associated with a wide range of psychiatric and neurological

disorders, such as major depressive disorder[26], bipolar disorder[27], attention deficit hyperactivity disorder[28], and Parkinson's disease[29].

While structure-function coupling has been extensively implicated in development, cognition, and clinical outcomes, few studies have explicitly examined the extent to which structure-function coupling reflects a group-common characteristic or varies across individuals. Prior studies have indicated that functional connectivity is equally dominated by stable group and individual factors[29], while structural connectivity exhibits less variability across participants[30]. This leads to the hypothesis that structure-function coupling may primarily reflect group characteristics rather than individual differences. The investigation by Zimmermann et al., which utilized three distinct datasets and four parcellation atlases for connectivity calculation, revealed that individual-specific effects in structure-function coupling were evident in only one instance, with a particular dataset and atlas[30]. This work evaluated the coupling using linear association, which solely accounts for direct structural connectivity and ignores indirect functional communications. This methodological limitation might account for the scarcity of significant individual-specific effects. Furthermore, there is marked information regarding the group and individual effects of the coupling that remains uncharacterized beyond the coarse finding in the prior work[30]. To this point, no study has quantified and explicitly contrasted the magnitudes of group-common and individual-specific effects of structure-function coupling, as previously did for functional networks[29]. Additionally, the prior work only examined structure-function coupling at the whole-brain level[30], and how the group and individual coupling effects organized at the cortical regional level remains unclear.

Here, we proposed to use graph neural networks (GNNs), which capture indirect and non-linear inter-regional functional communication on the structural connectome compared to linear models[15,31-33], to investigate the magnitude of group-common and individual-specific effects of the structure-function coupling at both global and regional levels. We tested the following three interrelated hypotheses: First, we hypothesized that the GNN would accurately predict functional connectivity from structural networks. We also hypothesized that this prediction would primarily be determined by higher-order network topology, as GNNs inherently operate on this concept[31]. Second, we hypothesized that structure-function coupling would mainly reflect group-common characteristics; however, there would still exist a significant amount of individual effect, given the implications of structure-function coupling in human individual differences[10,13]. Furthermore, we predicted that GNNs might better identify individual coupling effects compared to traditional linear association methods, since GNNs take into account indirect functional communications. Third, we hypothesized that both group and individual effects at the regional level would be distributed across the cortex along the canonical sensorimotor-association cortical axis[24], which is a convergent organizing principle unifying diverse neurobiological properties. Specifically, we expected that the group effects of regional structure-function coupling would be higher in the primary sensorimotor cortex due to relatively minor inter-individual variability in both structural and functional connectivity[34,35]. Conversely, we expected the individual-specific effects of coupling to be greater in the higher-order association cortex, where functional communication may have become untethered from genetic and anatomical constraints[36].

**Results**

We utilized two independent datasets, namely the Human Connectome Project (HCP)-young adult (HCP-YA, $n$ = 297, 137 males, aged 22–36 years)[37] and HCP-development (HCP-D, $n$ = 499, 237

males, aged 8–21 years)[38], to evaluate structure-function coupling. As illustrated in **Fig. 1a**, we first constructed the connectome of functional connectivity (FC) and structural connectivity (SC) for each participant using a priori Schaefer cortical parcellation atlas of 400 regions[39]. Based on the resting-state functional MRI (fMRI) data, FC was defined as the Pearson correlation coefficient between each pair of regional time series, resulting in a 400×400 symmetrical FC matrix for each participant. The matrix consisted of 79,800 unique elements, with each element denoted as an "edge" connecting two cortical regions. Fisher *r*-to-*z* was used to improve the normality of the FC edge strength. Using diffusion MRI data, we reconstructed whole-brain white matter tracts of individual participants using probabilistic fiber tractography with multi-shell, multi-tissue constrained spherical deconvolution (CSD)[40]. Anatomically constrained tractography (ACT)[41] and spherical deconvolution informed filtering of tractograms (SIFT)[42] have been applied to improve the biological accuracy of fiber reconstruction. For each participant, we quantified the number of streamlines connecting each pair of cortical regions using the Schaefer atlas to construct a structural connectome of the streamline counts. The edge weights of the SC matrices were log transformed.

To fully investigate the indirect functional communication and nonlinear association between structural and functional connectomes, we used a graph neural network (GNN) framework to capture structure-function coupling by predicting the empirical FC from the SC[33,43]. The GNN framework treats each FC edge as a higher-order communication through the SC between two corresponding nodes. Specifically, our GNN model employed a two-layer graph convolutional network[44], which takes the SC as the input and aggregates the two-hop neighboring SC for each node to construct its node embeddings. Subsequently, a two-layer multilayer perceptron takes each

pair of node embeddings as inputs to predict the connected FC (**Fig. 1a**). For both the HCP-YA and HCP-D datasets, we randomly split the participants into two subsets, with one as the training set and the other as the test set. We used the GNN model trained from the training set to predict FC in the test set. We defined the Pearson correlation between the predicted and empirical FC as the structure-function coupling for each participant in the test set. The subsequent GNN-based coupling analyses were restricted to the test set.

We present the group-averaged connectivity matrices of SC, empirical FC, and predicted FC from the GNN in the HCP-YA dataset as examples (**Fig. 1b**). The connectivity matrix was organized based on the large-scale functional network affiliations of the 400 cortical regions to the Yeo 7 networks[45], which consists of visual, somatomotor, dorsal attention, ventral attention, frontoparietal, limbic, and default mode networks. The predicted FC matrix was similar to the empirical FC matrix (**Fig. 1b**), suggesting the effectiveness of our GNN model. **Fig. S1** illustrates the empirical and predicted connectivity matrices of the HCP-D dataset.

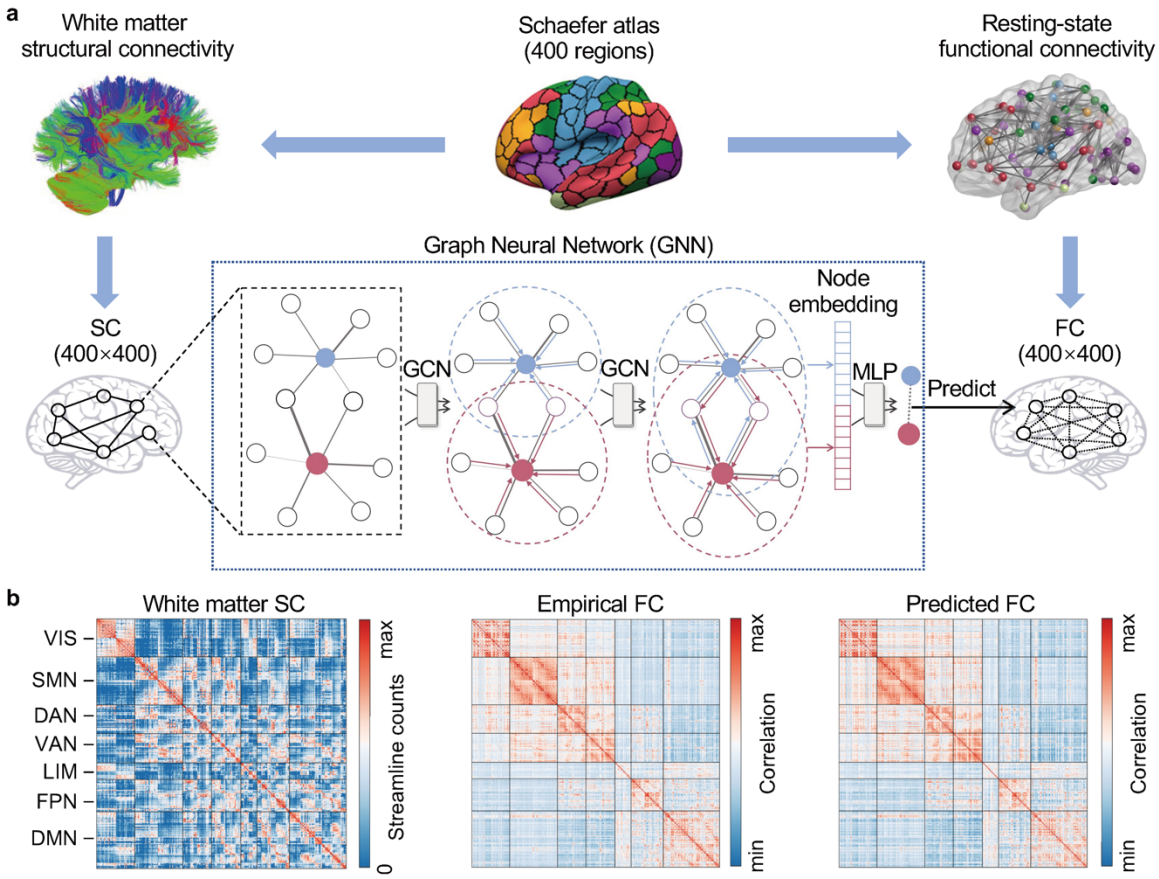


**Fig. 1 | The graph neural network (GNN)-based framework predicts functional connectivity from structural connectivity. a**, For each individual, the white matter structural connectivity (SC) and resting-state functional connectivity (FC) were constructed using the Schaefer-400 atlas. Both SC and FC can be characterized as a 400×400 matrix. We utilized a GNN model to predict FC from SC. Specifically, the GNN employs a two-layer graph convolutional network (GCN) to get the node embedding for each node and uses a two-layer multilayer perceptron (MLP) to predict each FC edge from the corresponding two node embeddings. **b**, The group-averaged connectivity matrix of SC, empirical FC, and predicted FC in the HCP-YA dataset. Visual inspection suggests a highly consistent connectional pattern between the empirical and predicted FC matrices. HCP-YA, Human Connectome Project (HCP)-young adult; VIS, visual network; SMN, somatomotor network; DAN, dorsal attention network; VAN, ventral attention network; LIM, limbic network; FPN, frontoparietal network; DMN, default mode network.

## GNN accurately captures the coupling between structural and functional network topology

Previous studies have consistently demonstrated robust coupling between SC and FC using linear associations[9-11]. In this study, we evaluated whether this was true in our datasets. We acquired group-average empirical FC and SC matrices and flattened the upper triangle elements into vectors

for both matrices. The linear association (Pearson correlation) demonstrated positive coupling between FC and SC across all edges with non-zero SC strength in both the HCP-YA ($r = 0.396$, $P < 1\times10^{-16}$; **Fig. 2a**) and HCP-D ($r = 0.420$, $P < 1\times10^{-16}$; **Fig. 2b**) datasets at the group level. These results are consistent with the previously reported magnitudes of group-level structure-function coupling using linear associations[10].

The linear association model only accounts for direct connections between nodes, while FC can emerge from polysynaptic communication on structural connectome[5,6]. A recent study indicated that a feed-forward fully-connected neural network accurately predicted FC from the SC with higher accuracy than coupling with a linear association. However, in this study, the network topology made a limited contribution to the prediction[46]. We extended these results by applying the GNN model to predict FC with SC, which has the potential to capture more information about structural network topology[31]. At the group level, the correlation between the predicted and empirical FCs was $r = 0.953$ ($P < 1\times10^{-16}$; **Fig. 2c**) for the HCP-YA and $r = 0.948$ ($P < 1\times10^{-16}$; **Fig. 2d**) for the HCP-D dataset. This result suggests that the GNN captured a much higher structure-function coupling than the linear association at the group level. Moreover, this group-level prediction accuracy was slightly higher than that of a fully-connected neural network, as reported in a previous study ($r = 0.9$)[15].

Next, we evaluated whether the GNN outperformed traditional approaches at the individual level. Using the linear association, we found that the correlation between FC and SC ranges from Pearson $r = 0.215$ to $r = 0.389$ ($r = 0.297 \pm 0.030$; **Fig. 2e**) across HCP-YA participants and ranges from $r = 0.215$ to $r = 0.409$ ($r = 0.306 \pm 0.028$; **Fig. 2f**) across HCP-D participants. In contrast, GNN

predicted FC from SC with an accuracy ranging from 0.514 to 0.782 ($r$ = 0.685 ± 0.046; **Fig. 2e**) across HCP-YA participants and from 0.451 to 0.752 ($r$ = 0.663 ± 0.047; **Fig. 2f**) across HCP-D participants. The lowest individual-level structure-function coupling from the GNN was higher than the highest coupling from the linear association in both datasets. Moreover, our individual-level prediction accuracy from the GNN was higher than that of a fully-connected deep neural network, as reported in prior work ($r$ = 0.55 ± 0.1)[15]. Overall, these results indicate that the GNN framework detected structure-function coupling better than a linear association and a traditional fully-connected neural network.

We further explored how network topology contributes to structure-function coupling. To do this, we rewired the SC to randomize the network topology while maintaining the distribution of the nodal degree and strength[47]. Using the linear association, we found that the coupling between FC and rewired SC was $r$ = 0.014 ± 0.006 (**Fig. 2e**) for HCP-YA participants and $r$ = 0.017 ± 0.006 (**Fig. 2f**) for HCP-D participants. To evaluate how the network topology contributed to the GNN-based structure-function coupling, we trained GNN models with rewired SC in the training data to predict the FC in the test data. Similarly, we found that GNN trained by rewired SC could only predict FC with an accuracy of $r$ = 0.308 ± 0.041 (**Fig. 2e**) for individual participants in HCP-YA and $r$ = 0.286 ± 0.029 (**Fig. 2f**) in HCP-D. Numerically, rewiring SC reduced the structure-function coupling by 55% (empirical: mean $r$ = 0.685, rewired: mean $r$ = 0.308) on average in HCP-YA, and by 57% (empirical: mean $r$ = 0.663, rewired: mean $r$ = 0.286) in HCP-D. As an alternative method to directly compare with one previous study[15], we retained the original SC in the training dataset to train the GNN model but rewired the SC in the test set. As a result, the prediction performance was $r$ = 0.041 ± 0.047 for testing participants in HCP-YA and $r$ = 0.025 ± 0.013 in

HCP-D. Therefore, rewiring the SC in the test set reduced the structure-function coupling by 94% (i.e., empirical: mean $r = 0.685$, rewired: mean $r = 0.041$) on average in HCP-YA and by 96% (i.e., empirical: mean $r = 0.662$, rewired: mean $r = 0.025$) in HCP-D. In contrast, a study using a fully-connected neural network reported that rewiring the SC in the test set reduced coupling by 20-50%[15]. This comparison indicates that our GNN captured more higher-order network topological information through coupling than the traditional fully-connected neural network. Overall, these results suggest that network topology drives structure-function coupling.

After demonstrating topology driven structure-function coupling at the global, whole-brain level, we evaluated structure-function coupling at the regional level for both the linear and GNN models. Specifically, the structural profile of each cortical region was defined as its connected SC edges for the linear model and its connected predicted FC edges for the GNN model. The functional profile of each cortical region was defined as the connected FC edges. Regional structure-function coupling was measured as the Pearson correlation between the structural and functional profiles for each cortical region. We found that the regional structure-function coupling ranged from 0.074 to 0.575 for HCP-YA (**Fig. 2g**) and from 0.065 to 0.640 for HCP-D (**Fig. 2h**) across all 400 cortical regions for the linear model. Using the GNN model, the regional structure-function coupling increased substantially, ranging from 0.326 to 0.809 for HCP-YA (**Fig. 2i**) and from 0.263 to 0.801 for HCP-D (**Fig. 2j**) across the cortical regions. Importantly, for both the linear and GNN models, regional structure-function coupling was heterogeneously distributed across the cortex, with a higher value in the primary sensorimotor cortices and a lower value in the higher-order association cortices. This cortical pattern of structure-function coupling is consistent with prior literature[10,11].

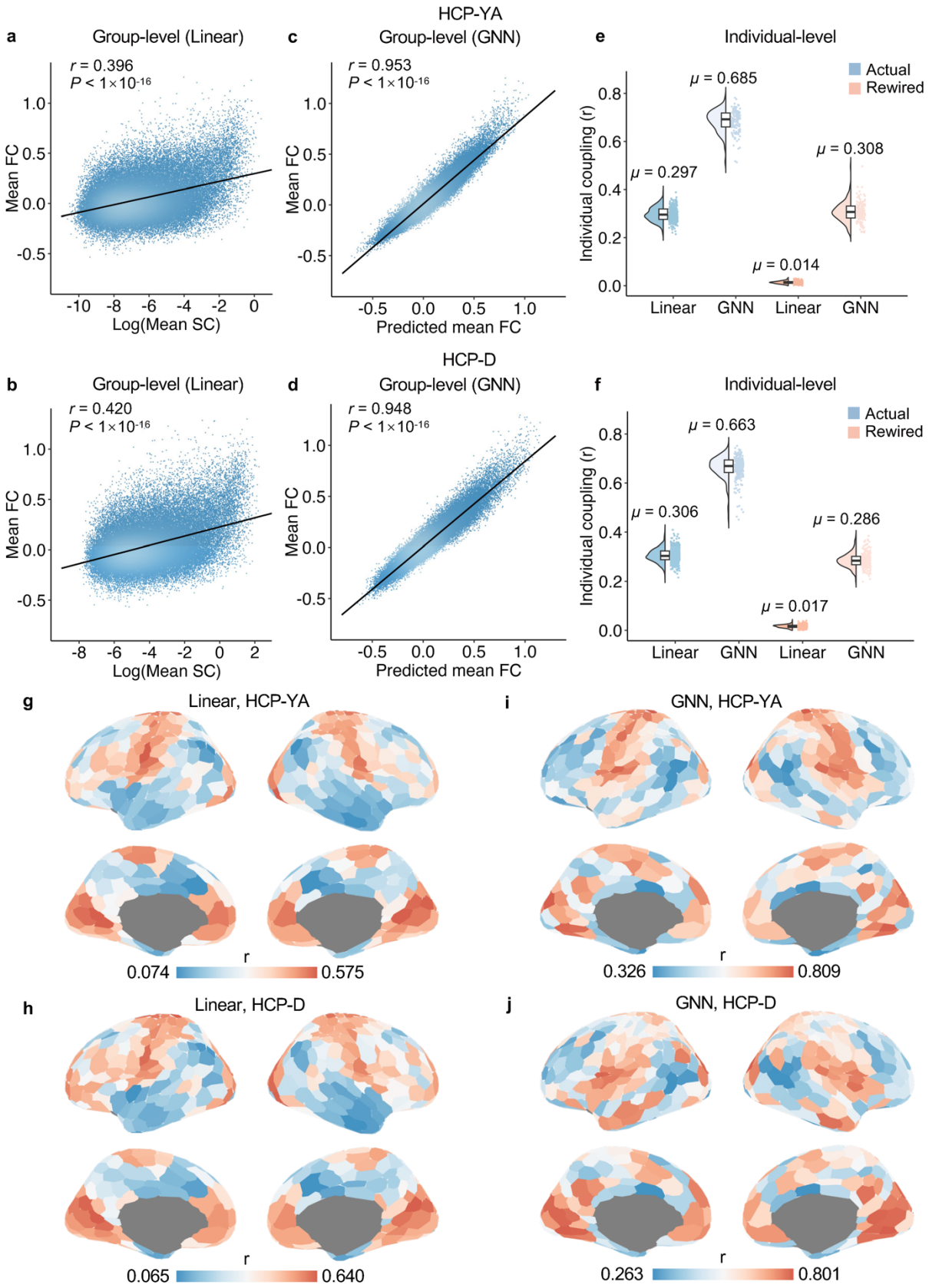
HCP-YA
a
Group-level (Linear)
r = 0.396
P < 1×10-16
Mean FC
Log(Mean SC)
c
Group-level (GNN)
r = 0.953
P < 1×10-16
Mean FC
Predicted mean FC
e
Individual-level
Actual
Rewired
Individual coupling (r)
μ = 0.297
μ = 0.685
μ = 0.014
μ = 0.308
Linear
GNN
Linear
GNN
HCP-D
b
Group-level (Linear)
r = 0.420
P < 1×10-16
Mean FC
Log(Mean SC)
d
Group-level (GNN)
r = 0.948
P < 1×10-16
Mean FC
Predicted mean FC
f
Individual-level
Actual
Rewired
Individual coupling (r)
μ = 0.306
μ = 0.663
μ = 0.017
μ = 0.286
Linear
GNN
Linear
GNN
g
Linear, HCP-YA
r
0.074
0.575
i
GNN, HCP-YA
r
0.326
0.809
h
Linear, HCP-D
r
0.065
0.640
j
GNN, HCP-D
r
0.263
0.801

**Fig. 2 | Structure-function coupling based on linear and GNN models. a**,**b**, The group mean SC was significantly correlated with mean FC in the HCP-YA (**a**, $r$ = 0.396, $P < 1\times10^{-16}$) and HCP-D (**b**, $r$ = 0.420, $P < 1\times10^{-16}$) datasets, based on the linear Pearson correlation. **c**,**d**, GNN accurately predicted the group mean FC from the mean SC in both datasets. The predicted mean FC was significantly correlated with mean empirical FC in the HCP-YA (**c**, $r$ = 0.953, $P < 1\times10^{-16}$) and HCP-D (**d**, $r$ = 0.948, $P < 1\times10^{-16}$) datasets. **e**,**f**, At the individual participant level, the GNN model returned a much higher structure-function coupling than linear association in both HCP-YA (**e**, linear: $r$ = 0.308 ± 0.041; GNN: $r$ =0.685 ± 0.046) and HCP-D (**f**, linear: $r$ = 0.286 ± 0.029; GNN: 0.663 ± 0.047) datasets. Moreover, rewiring the SC network by disrupting the network topology and keeping the degree and strength distribution substantially reduced individuals' structure-function coupling from both linear and GNN models in both HCP-YA (**e**, linear: $r$ = 0.014 ± 0.006; GNN: $r$ =0.308 ± 0.041) and HCP-D (**f**, linear: $r$ = 0.017 ± 0.006; GNN: 0.286 ± 0.029) datasets. This suggests that the structure-function coupling was mainly driven by the network topology. **g**,**h**, The regional structure-function coupling by linear association for HCP-YA (**g**) and HCP-D (**h**) datasets. **i**,**j**, The regional structure-function coupling by the GNN model for HCP-YA (**i**) and HCP-D (**j**) datasets.

**Structure-function coupling is primarily dominated by group-common effects, with subtle but significant individual-specific effects**

Having found that structure-function coupling was reliable and driven by network topology, we next examined the magnitudes of group-common and individual-specific effects in structure-function coupling, utilizing both linear and GNN models. To achieve this, we constructed a participant-by-participant matrix of structure-function coupling for both models. The diagonal elements of the matrix quantify the structure-function coupling within individuals, whereas the off-diagonal elements quantify the coupling between one participant's SC (or predicted FC when using the GNN) and another participant's FC (**Fig. 3a**). We designated the within-individual coupling as 'matched coupling' and the between-individual coupling as 'mismatched coupling'.

As expected, the average of all pairs of matched coupling (linear: HCP-YA: $r$ = 0.297; HCP-D: $r$ = 0.306; GNN: HCP-YA: $r$ = 0.685; HCP-D: $r$ = 0.663) was higher than the average of all pairs of mismatched couplings (linear: HCP-YA: $r$ = 0.294; HCP-D: $r$ = 0.302; GNN: HCP-YA: $r$ = 0.669;

HCP-D: $r = 0.646$) for both the linear and GNN models. We defined the total effects of structure-function coupling as the average matched coupling, group-common effects as the average mismatched coupling, and individual-specific effects as the difference between the average matched coupling and average mismatched coupling. A similar approach was used to evaluate group and individual effects in functional networks[29]. Using the linear model, our results revealed that individual effects accounted for 1.20% of the total effects of structure-function coupling in HCP-YA and 1.06% in HCP-D (**Fig. 3b**). By contrast, the individual effects of the GNN model accounted for 2.33% and 2.50% of the total effects in HCP-YA and HCP-D, respectively (**Fig. 3c**). These results indicate that the GNN outperformed the linear association in capturing individual effects, suggesting that some individual effects of structure-function coupling can be explained by the nonlinear high-order network topology. Moreover, both models demonstrated that structure-function coupling was primarily dominated by group-common factors (more than 97%) rather than individual-specific traits (less than 3%).

As the individual effects of structure-function coupling were minor for both models, we next evaluated whether the individual effects were statistically significant. To test this, we extracted the matched coupling and the average of all mismatched coupling for each participant (**Fig. 3d**). We compared matched coupling and average mismatched coupling across all participants using two-tailed paired t-tests. The results indicated that the matched coupling was significantly higher than the mismatched coupling in both the linear (HCP-YA: $P < 0.0001$; HCP-D: $P < 0.0001$; **Fig. 3e**) and GNN models (HCP-YA: $P < 0.0001$; HCP-D: $P < 0.0001$; **Fig. 3f**). These findings confirm that the individual effects of structure-function coupling were statistically significant, as demonstrated by two independent datasets and two distinct approaches.

Overall, our findings suggest that individual structure-function coupling primarily reflects group-common characteristics, with subtle yet significant individual-specific effects.

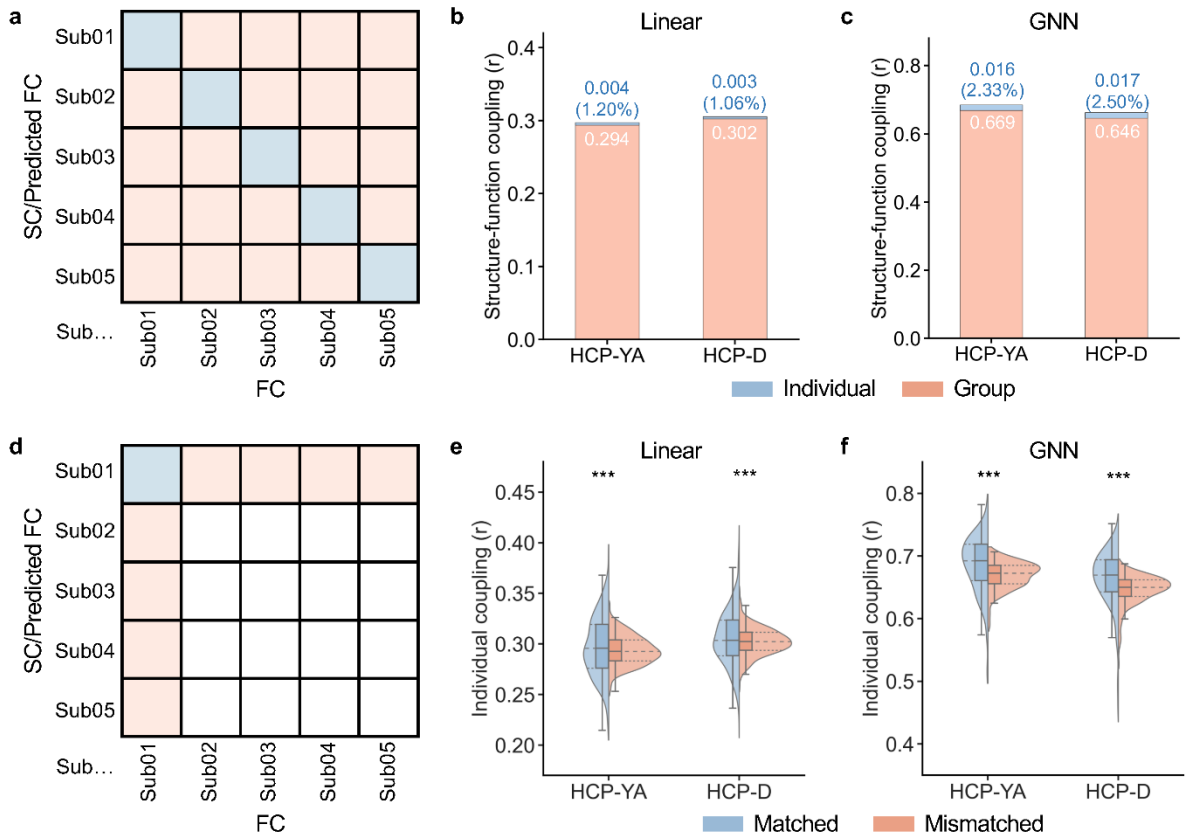


**Fig. 3 | The group-common and individual-specific effects of structure-function coupling. a**, The matrix of structure-function coupling between each pair of participants. Diagonal elements (cold color) represent the within-subject coupling (i.e., matched coupling), while off-diagonal elements (warm color) represent the coupling between one participant's SC or predicted FC and another participant's FC (i.e., mismatched coupling). SC was used for the linear model and the predicted FC was used for the GNN model to calculate the structure-function coupling. The total effects were defined as the average value of the diagonal elements; the group-common effects were defined as the average value of the off-diagonal elements; and the individual-specific effects were defined as their difference. **b**,**c**, The group and individual effects were estimated using the linear model (**b**, HCP-YA: 0.294/0.004; HCP-D: 0.302/0.003) and the GNN model (**c**, HCP-YA: 0.669/0.016; HCP-D: 0.646/0.017). **d**, The matched coupling and the average of all mismatched coupling were extracted for each participant and then were statistically compared across participants using two-tailed paired t-tests. **e**, **f**, The matched individual coupling was significantly higher than the mismatched coupling for both the linear (**e**) and the GNN models (**f**), suggesting

statistically significant individual-specific effects of structure-function coupling. *** indicates $P < 0.0001$, two-tailed paired t-test.

**Group and individual effects of structure-function coupling are organized on the cortex along the sensorimotor-association axis**

Having identified the magnitudes of group-common and individual-specific effects in structure-function coupling at the global level, we evaluated how group and individual effects were distributed across the cortex at the regional level. Recent studies have consistently demonstrated that the sensorimotor-association cortical axis is a unifying organizing principle for both the anatomical and functional properties across the cortex[24]. We hypothesized that the cortical distributions of both group and individual effects would align with the sensorimotor-association cortical axis. We acquired a priori cortical map of the sensorimotor-association cortical axis (**Fig. 4a**), which was derived by averaging diverse cortical neurobiological properties[24]. The cortical regions were continuously ranked along this axis, with the primary sensorimotor cortices representing the lowest ranks and higher-order association cortices representing the highest ranks.

We calculated the group and individual effects of the GNN-based structure-function coupling at the regional level. We constructed a participant-by-participant matrix of the GNN-based coupling and averaged all mismatched couplings for each cortical region, resulting in regional group effects. We observed that the group effects were higher in the primary sensorimotor cortices and lower in the higher-order association cortices in both the HCP-YA (**Fig. 4b**) and HCP-D (**Fig. 4c**) datasets. Using the Spearman rank correlation and a conservative spin-based spatial permutation test[48], we found that the cortical distributions of the regional group effects were highly reproducible between the two datasets (Spearman's rho = 0.86, $P_{spin} < 0.001$). Using the linear model to evaluate regional

structure-function coupling, we observed that the cortical distribution of group effects was similar to that using the GNN model in both the HCP-YA and HCP-D datasets (**Fig. S2a**).

Next, we quantitatively evaluated whether the group effects of the regional structure-function coupling were organized along the principal sensorimotor-association cortical axis. Using the Spearman correlation, we found that the group effects, based on the GNN model, were negatively correlated with the ranks of the sensorimotor-association axis across all cortical regions in both the HCP-YA (Spearman's rho = -0.48, $P_{spin} < 0.001$; **Fig. 4d**) and HCP-D (Spearman's rho = -0.30, $P_{spin} = 0.003$; **Fig. 4e**) datasets. The sensorimotor pole of the cortical axis showed a higher group effect, and the association pole showed a lower group effect. Additionally, using a linear model to evaluate structure-function coupling, we consistently observed a negative association between regional group effects and sensorimotor-association axis ranks in both HCP-YA (Spearman's rho = -0.54, $P_{spin} < 0.001$; **Fig. S2b**) and HCP-D (Spearman's rho = -0.50, $P_{spin} < 0.001$; **Fig. S2c**). These results suggest that the sensorimotor-association cortical axis potentially constrains the cortical distribution of the group effects of structure-function coupling.

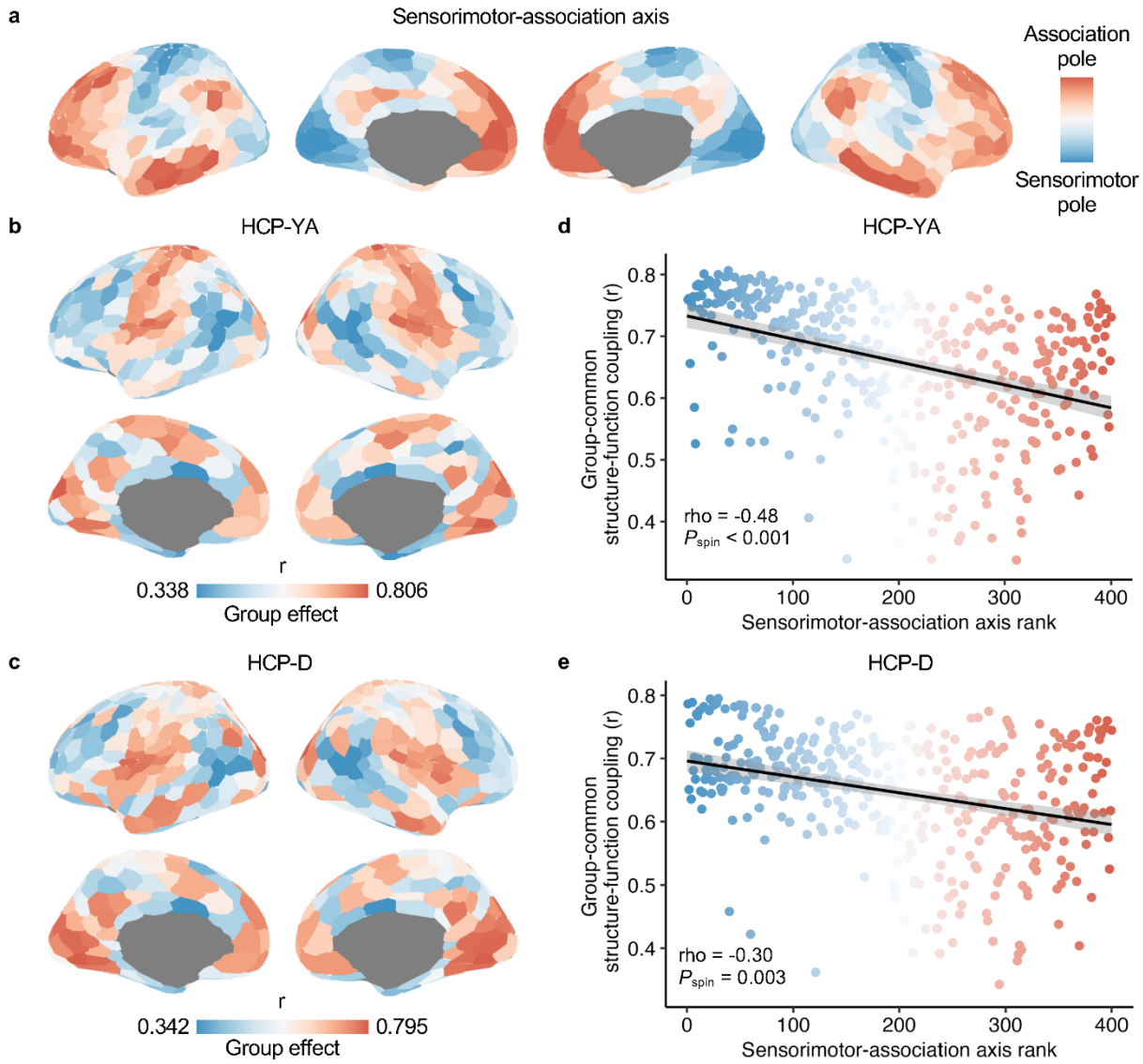


**Fig. 4 | GNN-derived regional group-common structure-function effects inversely align with the sensorimotor-association cortical axis. a**, The cortical map of the priori sensorimotor-association axis was derived from Sydnor et al.[24], where warm colors represent association cortices with higher ranks and cold colors represent sensorimotor cortices with lower ranks. **b**,**c**, The cortical map of group-common effects in regional structure-function coupling estimated by the GNN model in the HCP-YA (**b**) and HCP-D (**c**) datasets. **d**,**e**, The regional group effects of structure-function coupling were negatively correlated with the sensorimotor-association axis ranks in the HCP-YA (**d**, Spearman's rho = -0.48, $P_{spin} < 0.001$) and HCP-D (**e**, Spearman's rho = -0.30, $P_{spin} = 0.003$) datasets. The outliers (mean $\pm$ 3×SD) were excluded in the correlation analysis. Each point in the scatter plot represents a cortical region and is colored by its rank in the sensorimotor-association axis.

Next, we examined the cortical distribution of the individual-specific effects of regional structure-function coupling. Using regional participant-by-participant matrices of GNN-based structure-function coupling, we calculated individual effects as the difference between the average matched and mismatched coupling for each cortical region. We observed that individual-specific effects were weaker in the sensorimotor cortices and stronger in the association cortices in both the HCP-YA (**Fig. 5a**) and HCP-D (**Fig. 5b**) datasets. The cortical distribution of individual effects was significantly aligned between the two datasets (Spearman's rho = 0.48, $P_{spin} < 0.001$). Using the linear model, we observed a cortical pattern similar to that of the GNN model for both datasets (**Fig. S2d**).

By quantifying the alignment with the sensorimotor-association cortical axis, we found a significant positive correlation between the individual effects and the ranks of this cortical axis in both the HCP-YA (Spearman's rho = 0.28, $P_{spin} = 0.004$; **Fig. 5c**) and HCP-D (Spearman's rho = 0.34, $P_{spin} = 0.002$; **Fig. 5d**) datasets. These results indicate an opposite cortical pattern in individual-specific effects compared to group-common effects. The sensorimotor pole of the axis had a lower individual effect, and the association pole showed a higher individual effect. However, using the linear model, the association between regional individual effects and cortical axis rank was not significant in either the HCP-YA (Spearman's rho = 0.00, $P_{spin} = 0.510$; **Fig. S2e**) or HCP-D (Spearman's rho = -0.15, $P_{spin} = 0.127$; **Fig. S2f**) datasets. These results suggest that the GNN model is better at capturing biologically meaningful individual-specific effects of structure-function coupling in the human brain.

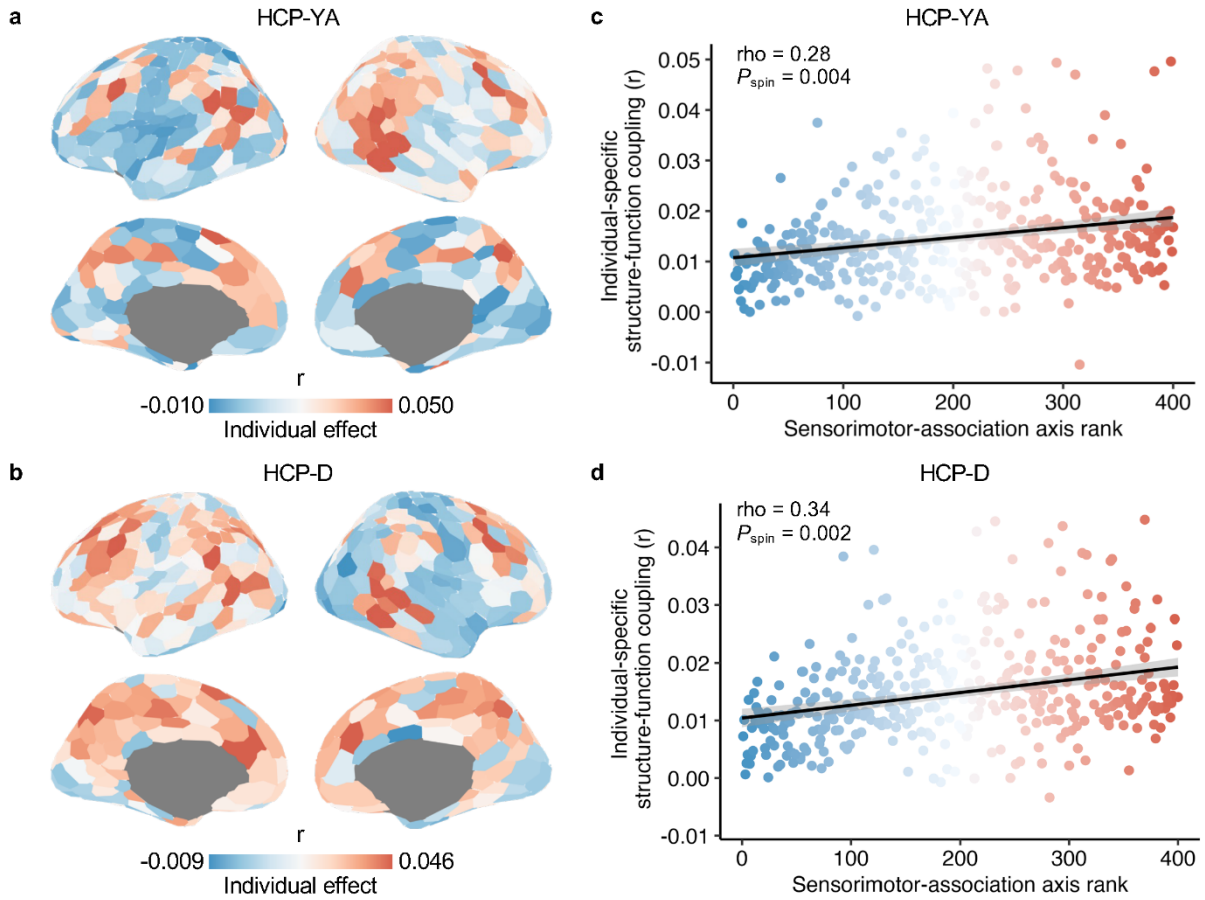


**Fig. 5 | GNN-derived regional individual-specific effects of structure-function positively align with the sensorimotor-association cortical axis. a**,**b**, The cortical map of individual-specific effects in structure-function coupling as estimated by the GNN model in the HCP-YA (**a**) and HCP-D (**b**) datasets. **c**,**d**, The individual-specific effects were positively correlated with the ranks in the sensorimotor-association axis across all cortical regions in the HCP-YA (**c**, Spearman's rho = 0.28, $P_{spin}$ = 0.004) and HCP-D (**d**, Spearman's rho = 0.34, $P_{spin}$ = 0.002) datasets. The outliers (mean $\pm$ 3 × SD) were excluded from the correlation analysis. Each point in the scatter plot represents a cortical region and is colored by its cortical axis rank.

## Sensitivity analyses

We performed two additional analyses to ensure that our results were robust to the methodological choices. In this study, we defined the individual effects of structure-function coupling by subtracting the average mismatched coupling (between-subject coupling) from the matched coupling (within-subject coupling). This measurement may be influenced by the magnitude of the

total effects, as larger total effects can potentially generate larger individual effects. To mitigate the potential scaling issue, we defined the normalized individual effects as the proportion of the individual effect to the total effect and re-evaluated the alignment between the normalized individual effects and the sensorimotor-association cortical axis ranks. Similar to our main results, we found that the normalized individual effects were lower in the sensorimotor cortices and higher in the association cortices (Fig. **S3a** & **S3b**). Moreover, we observed a significant positive correlation between individual effects and cortical axis rankings in the HCP-YA (Spearman's rho = 0.33, $P_{spin} < 0.001$; **Fig. S3c**) and HCP-D (Spearman's rho = 0.36, $P_{spin} = 0.001$; **Fig. S3d**) datasets.

We tested the robustness of our results with respect to brain parcellation. In the main analyses, we constructed SC and FC of the Schaefer-400 atlas[39]. Here, we validated our GNN model using another Schaefer-200 parcellation. We first confirmed the significance of individual-specific structure-function coupling effects. We observed significant individual effects of coupling with the Schaefer-200 (**Fig. S4a**). Furthermore, we demonstrated a negative association between group effects and the sensorimotor-association cortical axis ranks (**Fig. S4 b-d**), and a positive association between individual effects and cortical ranks (**Fig. S4 e-g**) across all regions. Overall, our main results are robust to the choice of cortical parcellation.

## Discussion

In this study, we proposed a graph neural network (GNN) framework to evaluate the magnitude of the group-common and individual-specific effects of structure-function coupling. We found that SC accurately predicted the FC of unseen individuals using the GNN model, and this prediction was driven by network topology. We observed that structure-function coupling was dominated by

group-common characteristics; simultaneously, minor individual-specific effects were also noted to be significant. Finally, we found that both regional group and individual effects were hierarchically patterned across the cortex along the fundamental sensorimotor-association cortical axis. The sensorimotor pole of the axis showed a higher group effect and lower individual effect, whereas the association pole showed a higher individual effect and lower group effect in structure-function coupling. These results were consistent for the two independent high-quality datasets. Our findings emphasize the importance of considering group and individual effects in individual difference studies of structure-function coupling.

Understanding the dynamic communication process in the structural connectome is a central goal in neuroscience[5,6]. Prior studies have demonstrated that the SC of macroscale white matter tracts is associated with FC, as measured by the correlation between pairs of regional time series[9-23,49]. The cortical distribution of regional structure-function coupling aligns with the axis of the fundamental sensorimotor-association cortical hierarchy[10,11,24]. Moreover, structure-function coupling changes with age and is related to individual differences in cognition and psychopathology[10,13,21,27,50]. Building on these studies, our work provides a systematic examination of the group-common and individual-specific effects of the structure-function coupling at the global and regional levels using both the linear association and advanced GNN.

Using the GNN framework, we found that SC reconstructed using diffusion MRI accurately predicted functional connectivity in unseen individuals using resting-state fMRI. Consistent with our results, previous studies have consistently demonstrated a robust coupling between SC and FC using a variety of interpretable models, such as linear associations[9-12], biophysical models[14],

communication models[6,13,20,22,51], and network control theory[52-55]. However, these interpretable models typically return relatively small structure-function coupling values, even when accounting for indirect communication, suggesting a potentially imperfect alignment between structural and functional connectivity[6,7,23]. Recently, Sarwar et al. found that a fully-connected neural network predicted FC with much higher accuracy than interpretable models[15], suggesting that structure-function coupling could be more significant than previously imagined. Two recent studies employed GNNs to investigate structure-function coupling; however, they did not evaluate how the network topology contributed to the coupling[33,43]. Our results extended these findings by demonstrating that the GNN achieved higher structure-function coupling than fully-connected neural networks, and this improvement was primarily attributed to the network topology. Specifically, by randomizing the network topology of SC, our GNN model reduced the prediction accuracy by more than 94%, whereas the fully-connected neural network reduced the prediction accuracy by 20-50%, as shown in a previous work[15]. This result demonstrates that prediction using a GNN is mainly driven by the network topology. Our results were also consistent with prior findings that GNNs are better at capturing topological representations of network data, such as cellular networks[56] and protein networks[57], than traditional deep learning approaches.

Our results also demonstrated that structure-function coupling was dominated by group-common effects, but the remaining minor individual effects were also significant. Robust group effects could underlie past successes in the estimation of structure-function coupling at the group level[9,11,14,16-19]. This result was also consistent with prior studies showing that functional networks were largely determined by the group-common organizational principle[29] and structural networks were even less variable than functional networks[30]. In direct support of our results, a recent study

also observed that structure-function coupling based on a linear association was dominated by group effects, which were consistent across six datasets with different acquisitions or processing methods[30]. However, individual effects of structure-function coupling were only observed in one of their six datasets[30]. Here, using an advanced GNN approach and two independent, high-quality datasets, we demonstrated that the individual effects of structure-function coupling were also robust and reproducible. Moreover, our results indicated that the individual effects with the GNN approach were much larger than those with the linear association approach, which potentially explained the nonstable individual effects in a previous study using linear association[30]. Future studies are warranted to examine how to improve interpretable network communication models to better detect the individual effects of structure-function coupling.

The sensorimotor-association cortical hierarchy has been proposed as a unifying cortical organizing principle for diverse neurobiological properties, including structure, function, metabolism, transcription, and evolution[10,11,18,24,58-63]. Recent studies have demonstrated that the cortical distribution of structure-function coupling aligns with the sensorimotor-association axis[10,11]. Consistent with these previous reports, we found that both the group and individual effects of regional structure-function coupling were hierarchically distributed across the cortex along the sensorimotor-association cortical axis. More specifically, we observed that the higher-order association cortex, which is located at the top end of the cortical axis, displayed the highest individual effects and lowest group effects, whereas the primary sensorimotor cortex displayed the highest group effects and lowest individual effects. Both structural and functional connectivity exhibited the highest inter-individual variability in the association cortex and the lowest in the sensorimotor cortex[34,35], which partly supports our findings. Moreover, the sensorimotor cortex

primarily comprises circuits with relatively simple and canonical feedforward and feedback connectivity patterns[64], which could potentially result in high cross-individual similarity in structure-function coupling. In contrast, the association cortex exhibits a non-canonical circuit architecture with complicated and distributed connections[65], which could lead to individual diversity in structure-function coupling.

This study has several potential limitations. First, precisely reconstructing individuals' white matter SC is challenging because of the inherent limitations of diffusion MRI-based fiber tractography. In this study, we used state-of-the-art probabilistic fiber tractography with multi-shell, multi-tissue constrained spherical deconvolution[40] and applied anatomically constrained tractography[41] and spherical deconvolution-informed filtering of tractograms[42] to improve biological accuracy. Moreover, consistency-based thresholding was used to reduce the influence of false-positive connections[10]. Second, the current study did not analyze the structure-function coupling of the subcortical and cerebellar structures, as these regions typically have a low signal-to-noise ratio (SNR) in fMRI data and require specialized analysis procedures that are different from those applied to the cortex. Future studies may evaluate the group and individual effects of structure-function coupling in the subcortical and cerebellar regions. Finally, although the GNN accurately predicted FC with structural network topology, its black-box nature prevented us from understanding the underlying communication mechanism supporting this prediction. However, this result provides a benchmark for optimizing interpretable models to explicitly explain how the structural connectome supports the functional connectivity.

Notwithstanding these limitations, we reliably demonstrated that the structure-function coupling is dominated by the group-common effects and the minor yet significant individual-specific effects using advanced GNN models. The individual coupling effects were the highest in the association cortex, which is related to the prolonged development of higher-order cognition and confers diverse psychopathologies[24]. This implies that structure-function coupling could be a potential neuromarker for tracking individual differences in cognitive development and vulnerability to mental disorders. However, the minor individual effects also suggest caution in interpreting the individual differences in structure-function coupling among individuals. As structural connectivity pathways facilitate the propagation of neurostimulation-induced activity[20,66], our findings may have implications for the clinical practice of neurostimulation. The dominant group effects in structure-function coupling could explain why the same neurostimulation target (i.e., dorsal lateral prefrontal cortex) has benefited many different patients[67]. Simultaneously, significant individual-specific effects could explain why personalized stimulation targets have improved intervention effects for certain patients[68].

## Methods

### HCP young adult (HCP-YA) dataset

We acquired multi-modal neuroimaging data from 339 unrelated participants (156 males, aged 22–37) from the HCP young adult (HCP-YA) dataset (release S900), including T1-weighted structural, resting-state functional MRI (fMRI) and diffusion MRI[37]. All imaging data were acquired by a multiband sequence on a Siemens 3T Skyra scanner. Two resting-state fMRI sessions, with two runs in each session (left-right and right-left phase-encoding), were acquired for each participant with a resolution of 3 mm isotropic. Each resting-state run comprised 1,200 frames for approximately 15 min in length. For diffusion MRI, data were acquired in two runs

with opposite phase-encoding directions for each participant. Each run included 270 non-collinear directions with 3 non-zero shells (b = 1000, 2000, and 3000 s/mm$^2$). Other details regarding the HCP-YA dataset and MRI acquisition parameters have been described in prior study[37].

**HCP development (HCP-D) dataset**

This study also comprised 633 participants (294 males, aged 8–21) obtained from the HCP-development (HCP-D) dataset (Release 2.0)[38]. All data were collected using a multiband EPI sequence on a 3T Siemens Prisma scanner. Two resting-state fMRI sessions were acquired for each participant, with two runs in each session, using anterior-posterior (AP) and posterior-anterior (PA) phase-encoding, respectively. Each resting-state run was approximately 6.5 min with 488 frames. Diffusion MRI data included two sessions, each with two non-zero shells (b = 1500, 3000 s/mm$^2$) and 185 diffusion-weighted directions. Further details about the HCP-D dataset have been described in previous study[38].

**Structural and functional MRI data processing**

Minimally preprocessed T1-weighted structural and functional MRI data were acquired from the HCP-D and HCP-YA datasets[69]. Briefly, structural MRI data were corrected for intensity non-uniformity, skull-stripped, and then used for cortical surface reconstruction. Volume-based structural images were segmented into cerebrospinal fluid (CSF), white matter, and gray matter, and spatially normalized to the standard MNI space. Functional MRI data were preprocessed with slice-timing, motion and distortion correction, co-registration to structural data, normalization to MNI space, and projection to cortical surface. Functional timeseries were resampled to FreeSurfer's fsaverage space, and grayordinates files containing 91k samples were generated.

We then followed the post-processed protocols of eXtensible Connectivity Pipelines (XCP-D; https://xcp-d.readthedocs.io/en/latest/)[70]. We regressed out 36 nuisance regressors from the BOLD time series, including six motion parameters, global signal, mean white matter signal, and mean CSF signal, along with their temporal derivatives, quadratic terms, and quadratic derivatives[71]. Residual timeseries were then band-pass filtered (0.01–0.08 Hz). We quantified head motion by calculating Jenkinson's framewise displacement (FD)[72], and we further reduced the potential effects of head motion by excluding subjects based on two criteria[73]. First, we dropped those fMRI runs that included more than 25% of the frames with FD > 0.2 mm. Second, we calculated the mean FD distribution for each fMRI run by pooling frames of all participants. Then, we derived the third quartile (Q3) and interquartile range (IQR) of this distribution. Runs with mean FD greater than 'Q3+1.5×IQR' were excluded. We excluded 111 HCP-D and 42 HCP-YA participants based on these two criteria. Additionally, seven participants from the HCP-D were excluded because of less than four resting-state fMRI runs. Consequently, 514 participants from the HCP-D and 297 participants from the HCP-YA datasets were included in subsequent analyses.

**Functional connectivity construction with functional MRI**

Functional connectivity (FC) refers to the temporal correlation of functional MRI signals. For HCP-YA and HCP-D datasets, we constructed FC by the following procedures. First, we extracted regional BOLD timeseries based on the a priori Schaefer parcellation with 400 parcels[39]. Next, FC was calculated as the Pearson correlation coefficient between each pair of regional BOLD timeseries, resulting in a 400×400 symmetrical FC matrix for each participant. We then applied Fisher's z-transformation to each FC value in the matrix. Finally, the 400 parcels were mapped

onto the seven intrinsic networks from Yeo atlas[45], including the visual network (VIS), somatomotor network (SMN), dorsal attention network (DAN), ventral attention network (VAN), frontoparietal network (FPN), limbic network (LIM), and default mode network (DMN).

**Diffusion MRI data processing**

We used minimally preprocessed diffusion MRI data from the HCP-YA dataset[37]. The minimal preprocessing pipeline comprises b0 image intensity normalization across runs, EPI distortion correction, eddy current and motion correction, gradient nonlinearity correction, and registration to the native structural space (1.25 mm). The processed diffusion MRI data were further corrected for B1 field inhomogeneity using MRtrix3. Diffusion MRI data from HCP-D were preprocessed by QSIPrep (https://qsiprep.readthedocs.io/), an integrative platform for preprocessing and reconstructing diffusion MRI data[74], including tools from MRtrix3 (https://www.mrtrix.org/)[75]. Prior to preprocessing, we concatenated the two AP runs and the two PA runs, respectively, and selected the frames with b-value < 100 s/mm$^2$ as the b0 image. Next, we applied MP-PCA denoising, Gibbs unringing, and B1 field inhomogeneity correction through MRtrix3's *dwidenoise*[76], *mrdegibbs*[77], and *dwibiascorrect*[78] functions. FSL's eddy was then used for head motion correction and Eddy current correction[79]. Finally, the preprocessed DWI timeseries was resampled to ACPC space at a resolution of 1.5 mm isotropic. Particularly, a total of 15 participants from the HCP-D were excluded from subsequent structural connectivity analyses due to incomplete DWI data (8 participants), tissue segmentation failure (5 participants), or the identification of isolated regions after tractography (2 participants). Therefore, a total of 297 participants from HCP-YA (137 males, aged 22–36) and 499 participants from HCP-D (237 males, aged 8–21) were analyzed in subsequent structure-function coupling analyses.

**White matter structural network construction with diffusion MRI**

We reconstructed whole-brain white matter tracts from preprocessed diffusion MRI data to construct the structural connectivity (SC). Reconstruction was conducted by the *mrtrix_multishell_msmt_ACT-hsvs* method in MRtrix3[75], which implements a multi-shell and multi-tissue constrained spherical deconvolution (CSD) to estimate the fiber orientation distribution (FOD) of each voxel[40]. Then, we followed the anatomically constrained tractography (ACT) framework to improve the biological accuracy of fiber reconstruction[41]. This tractography was performed by *tckgen*, which generates 40 million streamlines (length range from 30 to 250 mm, FOD power = 0.33) via a refined probabilistic streamlines tractography (iFOD2) based on the second-order integration over FOD. The streamlines were filtered from the tractogram based on the spherical deconvolution of the diffusion signal. We estimated the streamline weights using the command *tcksift2*[42]. Next, the SC matrix was constructed by *tck2connectome* based on the Schaefer-400 atlas for each participant. The edge weight of SC indicates the number of streamlines connecting two regions. For each connection, we normalized the edge weight by dividing the average volume of the corresponding two regions[80]. Furthermore, the edge weight of the SC matrix was log-transformed, which is commonly used to shift the non-Gaussian SC distribution to the Gaussian distribution in previous studies[7]. Finally, we obtained a 400×400 symmetric SC matrix for each participant. To address potential issues with spurious SC edges arising from probabilistic tractography[81], we adopted a group-consistency thresholding approach as in previous studies[10,82]. We calculated the coefficient of variation (CV) for edge weight across participants and subsequently applied a threshold to individual structural connectivity matrices at the 75th percentile for edge weight CV. The top quartile of inconsistent connections was removed.

**Predicting functional connectivity from structural connectivity using graph neural networks**

***Graph convolutional network.*** The main component of our graph neural network is the graph convolutional network (GCN)[44]. GCN generates node embeddings, representing the neighboring topological structure for each node. We denoted the node embedding generated from $l^{\text{th}}$ layer GCN as $\boldsymbol{H}^l \in \mathbb{R}^{N \times C_l}$, where $l \in \{1, \dots, L\}$ represents the layer index and $C_l$ represents the embedding dimension of layer $l$. $H^0$ is the exception representing the dimension of the input features of GCN. The input features are one-hot vectors that indicate the brain region of each node. Through message passing, the node embedding from the $l^{\text{th}}$ layer will pass along the network connectivity, denoted its adjacency matrix as $\boldsymbol{A}$, towards their neighboring nodes, convoluted by a GCN layer to get the node embedding of the $(l+1)^{\text{th}}$ layer. In our work, $\boldsymbol{A}$ is the adjacency matrix of SC, i.e., $\boldsymbol{A} \in \mathbb{R}^{K \times K}$. $K = 400$ is the number of nodes for the Schaefer-400 atlas. Therefore, the update equation of the node embedding from the $l^{\text{th}}$ layer to the $(l+1)^{\text{th}}$ layer is denoted as:

$$\boldsymbol{H}^{l+1} = \mathrm{GCN}(\boldsymbol{H}^l, \boldsymbol{A})$$

With $L$ layers in total, this message passing allows each node to embed its L-hop topological neighborhood. The concrete equation is formulated as:

$$\boldsymbol{H}^{l+1} = \mathrm{PReLU}(\widehat{\boldsymbol{D}}^{-\frac{1}{2}} \widehat{\boldsymbol{A}} \widehat{\boldsymbol{D}}^{\frac{1}{2}} \boldsymbol{H}^l \boldsymbol{W}^l_{\mathrm{GCN}})$$

where $\boldsymbol{W}^l_{\mathrm{GCN}} \in \mathbb{R}^{C_l \times C_{l+1}}$ is the trainable weight at the $l^{\text{th}}$ layer. $\widehat{\boldsymbol{A}}$ is the adjacency matrix with self-loop added, i.e., $\widehat{\boldsymbol{A}} = \boldsymbol{A} + \boldsymbol{I}_K$, where $\boldsymbol{I}_K \in \mathbb{R}^{K \times K}$ is the K-dimension identity matrix. $\widehat{\boldsymbol{D}}$ is the diagonal matrix, with the diagonal value $\widehat{D}_{ii}$ equals to the nodal strength of node $i$ in $\boldsymbol{A}$. As such, $\widehat{\boldsymbol{D}}^{-1/2} \widehat{\boldsymbol{A}} \widehat{\boldsymbol{D}}^{1/2}$ is the symmetric normalized Laplacian of the SC. We adopted the PReLU (Parametric Rectified Linear Unit) as the activation function due to its superior performance[83]:

$$\mathrm{PReLU}(x) = \begin{cases} x & x \geq 0 \\ \alpha x & x < 0 \end{cases}, \alpha \text{ is trainable}$$

***Multilayer perceptron.*** Subsequently, we used a pair of node embeddings as input to predict the functional connectivity between them by a two-layer multi-layer perceptron (MLP) with ReLU (Rectified Linear Unit) as the activation function (i.e., $\mathrm{ReLU}(x) = \max(0, x)$) after the first output layer. No activation function was used for the second layer. Specifically, for two node embeddings of node $i$ and $j$, represented by $h_i, h_j \in H$, the predicted FC, termed $\mathrm{pFC}_{ij} \in \mathbf{pFC}$, between them is calculated as:

$$\mathrm{pFC}_{ij} = \mathrm{MLP}\left(h_i\,, h_j, \boldsymbol{W}_{\mathrm{MLP}}\right) \in \mathbf{pFC}$$

***Model training and validation.*** To train our graph neural network model, we minimized the mean square error between the predicted FC and empirical FC with L2-regularizaion:

$$L_{\mathrm{MSE}} = \frac{1}{N_b} \sum_{n=1\ldots N_b} \frac{1}{M(M-1)} \sum_{i,j=1\ldots K;\, i\neq j} \left(\mathrm{pFC}_{ij} - \mathrm{eFC}_{ij}\right)^2 + \lambda\, |\boldsymbol{W}_{\mathrm{MLP}}|^2$$

where $\mathrm{eFC}_{ij} \in \mathbf{eFC}$ is the empirical FC between node $i$ and $j$. We adopted L2-regularization on the MLP's weights with regularization parameter $\lambda$. We trained the model through batched gradient descent with a batch of $N_b$ subjects and the Adam optimizer[84]. In addition, since FC is a symmetric matrix, we employed the $(\mathrm{pFC}_{ij} + \mathrm{pFC}_{ji})/2$ as the final predicted FC between node $i$ and $j$ for testing and further analysis. For both datasets, we randomly split 50% of the subjects as the training set, with the remaining 50% for testing and subsequent structure-function coupling analysis. By grid search based on the model's performance for 5-fold cross validation on the training set, we set the hyperparameter as: layer number (L=2), dimension for GCN (400×256×256), dimension for MLP (512×64×1), batch size (2), learning rate (0.0001), regularization parameter ($\lambda$=0.0001), and training epochs (400). The graph network model was

built and trained using Pytorch and PyTorch Geometric. More details about implementations could be found in the code repository at https://github.com/CuiLabCIBR/GNN_SC_FC.

**Structure-function coupling measured by linear and GNN models**

In this work, we evaluated the structure-function coupling using both a linear model and our proposed GNN model. The linear model assesses the Pearson correlation between SC and FC, focusing solely on direct connections with nonzero edge strength. However, functional connectivity can emerge from polysynaptic communication on structural connectome[5,6]. The GNN has the capability to capture both direct and indirect functional communications based on the sparse SC. For each dataset, all participants were split into two subsets with one used as training and another used as test set. The GNN model trained on all participants in the training set was used to predict the FC for the testing participants with their SC as input. The structure-function coupling was calculated as the Pearson correlation between the predicted and empirical FC for each participant in the test set. At the group level, we used the model from training data and all testing participants' average SC as input to predict the average FC. We calculated the Pearson correlation between the predicted and empirical average FC as the structure-function coupling at the group level.

We also estimated the structure-function coupling at both the whole-brain and regional levels. At the whole-brain level, we extracted the upper triangle elements (79,800 unique edges) from either the 400×400 SC matrix or the predicted FC matrix, creating a structural profile vector. Simultaneously, we extracted the upper triangle elements from the empirical FC matrix, forming a functional profile vector. We calculated the Pearson correlation between the structural profile

and functional profile across all connections at the global level. At the regional level, we first defined the regional structural and functional profiles. For the $i^{\text{th}}$ cortical region, we defined its structural or functional profile as the connections to all other cortical regions, which were represented by the $i^{\text{th}}$ row (399×1) from the connection matrix. The regional structure-function coupling was determined by calculating the Pearson correlation between the structural profile and functional profile of each cortical region, enabling us to generate a cortical map of regional structure-function coupling for both the linear and GNN models. Notably, all participants were involved and analyzed in the linear model based coupling, whereas the structure-function coupling based on the GNN model was derived from the test set, comprising 50% of the participants.

**Calculating group-common and individual-specific effects in structure-function coupling**

A previous study indicated that the individual FC is contributed by both group-common and stable individual-specific factors[29]. Following a similar approach, we aimed to distinguish between group-common and individual-specific effects in structure-function coupling using both linear and GNN models. To achieve this, we computed the structure-function coupling both within-individual and between each pair of different participants, resulting in a participant-by-participant asymmetrical matrix of structure-function coupling (**Fig. 3a**). In this matrix, the element in the $i^{\text{th}}$ row (SC or predicted FC from subject *i*) and $j^{\text{th}}$ column (FC from subject *j*), termed as $\text{cp}_{i,j}$, represents the structure-function coupling between the $i^{\text{th}}$ and $j^{\text{th}}$ participants. The diagonal elements of the matrix measure the structure-function coupling within individual, while the off-diagonal elements estimate the coupling between one individual's SC and another individual's FC. We referred to the within-individual coupling and between-individual coupling as 'matched coupling' and 'mismatched coupling', respectively. In this study, we treated the averaged between-

individual coupling as a group-common variance in the coupling across populations. This strategy has been used in a prior study of effects in function networks[29]. We supposed that the total effects of within-individual coupling encompass both group-common and individual-specific effects. Therefore, we defined the group-common and individual-specific effects of structure-function coupling as follows:

$$\mathrm{cp}_{\mathrm{group}} = \frac{1}{N(N-1)} \sum_{i,j=1\ldots N;\, i\neq j} \mathrm{cp}_{i,j}$$

$$\mathrm{cp}_{\mathrm{individual}} = \frac{1}{N} \sum_{i=1\ldots N} \mathrm{cp}_{i,i} - \mathrm{cp}_{\mathrm{group}}$$

where $N$ corresponds to the number of participants. Given our finding that individual structure-function coupling is primarily dominated by the group-common effect, with minor individual-specific effects (see **Results**), we proceeded to assess the statistical significance of these individual effects. For this purpose, we defined the matched coupling and mismatched coupling for each subject (**Fig. 3d**). Specifically, the mismatched coupling of subject $i$ was defined by the averaged coupling from all elements in the $i^{\mathrm{th}}$ row (SC or predicted FC from subject $i$, FC from other subjects) and $i^{\mathrm{th}}$ column (FC from subject $i$, SC or predicted FC from other subjects), except the within-individual coupling. The matched and mismatched coupling for each subject $i$ is defined as:

$$\mathrm{cp}_{\mathrm{match},i} = \mathrm{cp}_{i,i}$$

$$\mathrm{cp}_{\mathrm{mismatch},i} = \frac{1}{2(N-1)} \sum_{j=1\ldots N;\, j\neq i} \left(\mathrm{cp}_{i,j} + \mathrm{cp}_{j,i}\right)$$

We considered the individual-specific coupling effects significant if matched coupling were statistically higher than mismatched coupling across participants. We conducted a two-sided

paired t-test to examine the differences between matched coupling and mismatched coupling across all participants.

These analyses of group and individual effects in the coupling were first performed at the global level and then applied to each cortical region. It is noteworthy that only nonzero edges were examined in the linear model for both whole-brain and regional analyses.

**Alignment between cortical maps of group and individual effects of structure-function coupling and the sensorimotor-association cortical axis**

The sensorimotor-association axis has been consistently reported as a unifying organizing principle of both anatomical and functional properties across the cortex[24]. A previous study has also identified a negative association between structure-function coupling and sensorimotor-association axis rank[10]. Here, we further investigated how group-common and individual-specific coupling aligns with the sensorimotor-association cortical axis, respectively. We acquired a cortical map of the sensorimotor-association axis parcellated with the Schaefer-400 atlas from Sydnor et al.[24]. Cortical regions were continuously ranked along this axis, with the primary sensorimotor cortices representing the lowest ranks and the higher-order association cortices representing the highest ranks. For both linear and GNN models, we calculated Spearman's rank correlation to assess the alignment between the sensorimotor-association cortical axis and regional group-common effects as well as individual-specific effects across all cortical regions.

**Null models**

***Rewiring networks.*** To evaluate the contribution of network topology in structure-function coupling, we utilized the Maslov-Sneppen rewiring algorithm to rewire individual SC[85]. This process retained fundamental topological properties such as nodal degree and strength while randomizing topological structure. Furthermore, rewired networks preserved inter-node communication without creating isolated nodes. This algorithm was implemented via the Python version of the Brain Connectivity Toolbox (https://github.com/aestrivex/bctpy)[86]. For the linear model, we rewired SC from all individuals and re-evaluated the Pearson correlation between the rewired SC and FC for each participant. For the GNN model, we employed two strategies to assess the impact of network topology. Firstly, we aimed to evaluate how much the GNN model could learn from the higher-order topology, so we only rewired SC in training data to acquire a topological-null GNN model. We did not rewire the SC in the test set. We next used this topological-null GNN model to predict FC from SC in the test set. Then, we re-evaluated the Pearson correlation between the predicted FC and FC for each participant in the test set. Secondly, we trained the GNN model with the original SC and utilized the rewired SC to predict FC in the test set. We again re-evaluated the Pearson correlation between the predicted FC and FC for each participant in the test set. This strategy aimed to directly compare the contribution of the SC topology to our GNN with its contribution to the fully-connected network in a prior study[15].

***Spin test.*** We employed the spin test to evaluate the significance of the spatial correspondence between group-common and individual-specific effects of structure-function coupling and sensorimotor-association cortical axis[48]. Particularly, the spin test generated a null distribution by randomly rotating brain maps while maintaining the original spatial covariance structure[48]. This approach projected the group and individual effects onto a spherical cortical surface of the

FreeSurfer's fsaverage space and then randomly rotated 10,000 times to generate a list of rotated maps. Next, we calculated Spearman's rank correlation between each rotated map and the sensorimotor-association axis map to construct a null distribution. The $P$ value ($P_{spin}$) was determined by calculating the ratio of instances whose null correlations exceeded the empirical correlation coefficients.

**Sensitivity analyses**

One main result of this study is that the individual-specific effects of structure-function coupling showed a hierarchical pattern across the cortex that positively aligned with the sensorimotor-association cortical axis. However, as individual-specific effects are derived by subtracting the group-common effects from the total effects of the coupling, larger total effects might numerically lead to larger individual-specific effects. To address this potential scaling issue, we defined the 'normalized individual effect' by dividing the individual effect by the total regional structure-function coupling, representing the proportion of the individual effect to the total effect. Subsequently, we reevaluated the alignment between the normalized individual effects and the ranks of the sensorimotor-association cortical axis for the GNN model.

We also assessed the robustness of our main results to another cortical parcellation. In addition to the Schaefer atlas comprising 400 cortical regions used in our primary analyses, we validated our GNN models using the Schaefer atlas with 200 cortical regions[39]. First, we constructed the connectome of FC and SC for each participant using the Shcaefer-200 and retrained the GNN model. Then, we distinguished the group-common and individual-specific effects of structure-function coupling, and verified the significance of individual-specific effects with Schaefer-200.

Finally, we obtained the cortical maps of group-common and individual-specific effects of structure-function coupling and re-evaluated their alignment with the sensorimotor-association cortical axis. Specifically, leveraging the vertex-wise surface map of the sensorimotor-association axis in the fsLR-32k space[24], we computed the parcel-level sensorimotor-association axis rank values of Schaefer-200 by averaging rank values from all vertices within each parcel.

## Data availability

The HCP-YA and HCP-D datasets are available at https://db.humanconnectome.org/.

## Code availability

All code used to perform the analyses in this study can be found at https://github.com/CuiLabCIBR/GNN_SC_FC.


## Acknowledgements

This work is supported by the STI 2030-Major Projects (2022ZD0211300), Beijing Nova Program (Z211100002121002), and CIBR funds. Data were provided [in part] by the Human Connectome Project, WU-Minn Consortium (Principal Investigators: David Van Essen and Kamil Ugurbil; 1U54MH091657) funded by the 16 NIH Institutes and Centers that support the NIH Blueprint for Neuroscience Research; and by the McDonnell Center for Systems Neuroscience at Washington University. The HCP-Development 2.0 Release data used in this report came from DOI: 10.15154/1520708. Research reported in this publication was supported by the National Institute of Mental Health of the National Institutes of Health under Award Number U01MH109589 and by funds provided by the McDonnell Center for Systems Neuroscience at Washington University in St. Louis.


## Author contributions

Z.C. and P.C. designed the study. P.C. and H.Y. performed the analyses with support from T.S.O. H.Y. and X.X. completed data preprocessing. X.Z., H.J. and J.H. replicated the model training and

testing. H.Y and P.C. created the figures. Z.C. and T.S.O. supervised the project. R.C. provided resources. P.C., H.Y., and Z.C. wrote the manuscript with review and editing from all other authors.

**Competing interests**

The authors declare no competing interests.

## References


1 Sporns, O. The human connectome: a complex network. *Ann N Y Acad Sci* **1224**, 109-125 (2011). https://doi.org:10.1111/j.1749-6632.2010.05888.x

2 Bassett, D. S. & Bullmore, E. Small-world brain networks. *The Neuroscientist : a review journal bringing neurobiology, neurology and psychiatry* **12**, 512-523 (2006). https://doi.org:10.1177/1073858406293182

3 Sporns, O. & Betzel, R. F. Modular Brain Networks. *Annu Rev Psychol* **67**, 613-640 (2016). https://doi.org:10.1146/annurev-psych-122414-033634

4 van den Heuvel, M. P. & Sporns, O. Network hubs in the human brain. *Trends in cognitive sciences* **17**, 683-696 (2013). https://doi.org:10.1016/j.tics.2013.09.012

5 Avena-Koenigsberger, A., Misic, B. & Sporns, O. Communication dynamics in complex brain networks. *Nat Rev Neurosci.* **19**, 17-33 (2017). https://doi.org:10.1038/nrn.2017.149

6 Seguin, C., Sporns, O. & Zalesky, A. Brain network communication: concepts, models and applications. *Nature reviews. Neuroscience* (2023). https://doi.org:10.1038/s41583-023-00718-5

7 Suárez, L. E., Markello, R. D., Betzel, R. F. & Misic, B. Linking Structure and Function in Macroscale Brain Networks. *Trends in cognitive sciences* **24**, 302–315 (2020). https://doi.org:10.1016/j.tics.2020.01.008

8 Lynn, C. W. & Bassett, D. S. The physics of brain network structure, function and control. *Nature Reviews Physics* **1**, 318-332 (2019).

9 Honey, C. J. *et al.* Predicting human resting-state functional connectivity from structural connectivity. *Proceedings of the National Academy of Sciences of the United States of America* **106**, 2035-2040 (2009). https://doi.org:10.1073/pnas.0811168106

10 Baum, G. L. *et al.* Development of structure-function coupling in human brain networks during youth. *Proc Natl Acad Sci U S A* **117**, 771-778 (2020). https://doi.org:10.1073/pnas.1912034117

11 Vazquez-Rodriguez, B. *et al.* Gradients of structure-function tethering across neocortex. *Proc Natl Acad Sci U S A* **116**, 21219-21227 (2019). https://doi.org:10.1073/pnas.1903403116

12 Gu, Z., Jamison, K. W., Sabuncu, M. R. & Kuceyeski, A. Heritability and interindividual variability of regional structure-function coupling. *Nat Commun* **12**, 4894 (2021). https://doi.org:10.1038/s41467-021-25184-4

13 Zamani Esfahlani, F., Faskowitz, J., Slack, J., Misic, B. & Betzel, R. F. Local structure-function relationships in human brain networks across the lifespan. *Nat Commun* **13**, 2053 (2022). https://doi.org:10.1038/s41467-022-29770-y

14 Deco, G. *et al.* Resting-state functional connectivity emerges from structurally and dynamically shaped slow linear fluctuations. *The Journal of neuroscience : the official journal of the Society for Neuroscience* **33**, 11239-11252 (2013). https://doi.org:10.1523/JNEUROSCI.1091-13.2013

15 Sarwar, T., Tian, Y., Yeo, B. T. T., Ramamohanarao, K. & Zalesky, A. Structure-function coupling in the human connectome: A machine learning approach. *Neuroimage* **226**, 117609 (2021). https://doi.org:10.1016/j.neuroimage.2020.117609

16 Misic, B. *et al.* Network-Level Structure-Function Relationships in Human Neocortex. *Cereb Cortex* **26**, 3285-3296 (2016). https://doi.org:10.1093/cercor/bhw089
17 Suárez, L. E., Richards, B. A., Lajoie, G. & Misic, B. Learning function from structure in neuromorphic networks. *Nature Machine Intelligence* **3**, 771-786 (2021).
18 Demirtas, M. *et al.* Hierarchical Heterogeneity across Human Cortex Shapes Large-Scale Neural Dynamics. *Neuron* **101**, 1181-1194 e1113 (2019). https://doi.org:10.1016/j.neuron.2019.01.017
19 Misic, B. *et al.* Cooperative and Competitive Spreading Dynamics on the Human Connectome. *Neuron* **86**, 1518-1529 (2015). https://doi.org:10.1016/j.neuron.2015.05.035
20 Seguin, C. *et al.* Communication dynamics in the human connectome shape the cortex-wide propagation of direct electrical stimulation. *Neuron* **111**, 1391-1401 e1395 (2023). https://doi.org:10.1016/j.neuron.2023.01.027
21 Medaglia, J. D. *et al.* Functional Alignment with Anatomical Networks is Associated with Cognitive Flexibility. *Nat Hum Behav* **2**, 156-164 (2018). https://doi.org:10.1038/s41562-017-0260-9
22 Betzel, R. F. *et al.* Structural, geometric and genetic factors predict interregional brain connectivity patterns probed by electrocorticography. *Nat Biomed Eng* **3**, 902-916 (2019). https://doi.org:10.1038/s41551-019-0404-5
23 Valk, S. L. *et al.* Genetic and phylogenetic uncoupling of structure and function in human transmodal cortex. *Nat Commun* **13**, 2341 (2022). https://doi.org:10.1038/s41467-022-29886-1
24 Sydnor, V. J. *et al.* Neurodevelopment of the association cortices: Patterns, mechanisms, and implications for psychopathology. *Neuron* **109**, 2820-2846 (2021). https://doi.org:10.1016/j.neuron.2021.06.016
25 Feng, G. *et al.* Spatial and temporal pattern of structure-function coupling of human brain connectome with development. *bioRxiv*, 2023.2009. 2011.557107 (2023).
26 Soman, S. M. *et al.* Cortical structural and functional coupling during development and implications for attention deficit hyperactivity disorder. *Transl Psychiatry* **13**, 252 (2023). https://doi.org:10.1038/s41398-023-02546-8
27 Jiang, X. *et al.* Connectome analysis of functional and structural hemispheric brain networks in major depressive disorder. *Transl Psychiatry* **9**, 136 (2019). https://doi.org:10.1038/s41398-019-0467-9
28 Zarkali, A. *et al.* Organisational and neuromodulatory underpinnings of structural-functional connectivity decoupling in patients with Parkinson's disease. *Commun Biol* **4**, 86 (2021). https://doi.org:10.1038/s42003-020-01622-9
29 Gratton, C. *et al.* Functional Brain Networks Are Dominated by Stable Group and Individual Factors, Not Cognitive or Daily Variation. *Neuron* **98**, 439-452 e435 (2018). https://doi.org:10.1016/j.neuron.2018.03.035
30 Zimmermann, J., Griffiths, J., Schirner, M., Ritter, P. & McIntosh, A. R. Subject specificity of the correlation between large-scale structural and functional connectivity. *Netw Neurosci* **3**, 90-106 (2019). https://doi.org:10.1162/netn_a_00055
31 Zhou, J. *et al.* Graph neural networks: A review of methods and applications. *AI open* **1**, 57-81 (2020).

32 Neudorf, J., Kress, S. & Borowsky, R. Structure can predict function in the human brain: a graph neural network deep learning model of functional connectivity and centrality based on structural connectivity. *Brain Struct Funct* **227**, 331-343 (2022). https://doi.org:10.1007/s00429-021-02403-8

33 Hong, Y. *et al.* Structural and functional connectome relationships in early childhood. *Developmental Cognitive Neuroscience* **64**, 101314 (2023). https://doi.org:10.1016/j.dcn.2023.101314

34 Mueller, S. *et al.* Individual variability in functional connectivity architecture of the human brain. *Neuron* **77**, 586-595 (2013). https://doi.org:10.1016/j.neuron.2012.12.028

35 Huang, W. *et al.* Individual Variability in the Structural Connectivity Architecture of the Human Brain. *bioRxiv*, 2023.2001. 2011.523683 (2023).

36 Buckner, R. L. & Krienen, F. M. The evolution of distributed association networks in the human brain. *Trends Cogn Sci* **17**, 648-665 (2013). https://doi.org:10.1016/j.tics.2013.09.017

37 Van Essen, D. C. *et al.* The WU-Minn Human Connectome Project: An overview. *NeuroImage* **80**, 62-79 (2013). https://doi.org:10.1016/j.neuroimage.2013.05.041

38 Somerville, L. H. *et al.* The Lifespan Human Connectome Project in Development: A large-scale study of brain connectivity development in 5-21 year olds. *NeuroImage* **183**, 456-468 (2018). https://doi.org:10.1016/j.neuroimage.2018.08.050

39 Schaefer, A. *et al.* Local-Global Parcellation of the Human Cerebral Cortex from Intrinsic Functional Connectivity MRI. *Cerebral Cortex* **28**, 3095-3114 (2018). https://doi.org:10.1093/cercor/bhx179

40 Jeurissen, B., Tournier, J.-D., Dhollander, T., Connelly, A. & Sijbers, J. Multi-tissue constrained spherical deconvolution for improved analysis of multi-shell diffusion MRI data. *NeuroImage* **103**, 411-426 (2014). https://doi.org:10.1016/j.neuroimage.2014.07.061

41 Smith, R. E., Tournier, J.-D., Calamante, F. & Connelly, A. Anatomically-constrained tractography: improved diffusion MRI streamlines tractography through effective use of anatomical information. *NeuroImage* **62**, 1924-1938 (2012). https://doi.org:10.1016/j.neuroimage.2012.06.005

42 Smith, R. E., Tournier, J.-D., Calamante, F. & Connelly, A. SIFT2: Enabling dense quantitative assessment of brain white matter connectivity using streamlines tractography. *NeuroImage* **119**, 338-351 (2015). https://doi.org:10.1016/j.neuroimage.2015.06.092

43 Neudorf, J., Kress, S. & Borowsky, R. Structure can predict function in the human brain: a graph neural network deep learning model of functional connectivity and centrality based on structural connectivity. *Brain Structure and Function* **227**, 331-343 (2022). https://doi.org:10.1007/s00429-021-02403-8

44 Kipf, T. N. & Welling, M. Semi-Supervised Classification with Graph Convolutional Networks. (2017). https://doi.org:10.48550/arXiv.1609.02907

45 Thomas Yeo, B. T. *et al.* The organization of the human cerebral cortex estimated by intrinsic functional connectivity. *Journal of Neurophysiology* **106**, 1125-1165 (2011). https://doi.org:10.1152/jn.00338.2011

46 Rousselet, G. A., Pernet, C. R. & Wilcox, R. R. The percentile bootstrap: a primer with step-by-step instructions in R. *Advances in Methods and Practices in Psychological Science* **4**, 2515245920911881 (2021).

47 Vasa, F. & Misic, B. Null models in network neuroscience. *Nature reviews. Neuroscience* (2022). https://doi.org:10.1038/s41583-022-00601-9

48 Alexander-Bloch, A. F. *et al.* On testing for spatial correspondence between maps of human brain structure and function. *Neuroimage* **178**, 540-551 (2018). https://doi.org:10.1016/j.neuroimage.2018.05.070

49 Hermundstad, A. M. *et al.* Structural foundations of resting-state and task-based functional connectivity in the human brain. *Proceedings of the National Academy of Sciences of the United States of America* **110**, 6169-6174 (2013). https://doi.org:10.1073/pnas.1219562110

50 Jiang, H. *et al.* Structural-functional decoupling predicts suicide attempts in bipolar disorder patients with a current major depressive episode. *Neuropsychopharmacology* **45**, 1735-1742 (2020). https://doi.org:10.1038/s41386-020-0753-5

51 Seguin, C., Mansour, L. S., Sporns, O., Zalesky, A. & Calamante, F. Network communication models narrow the gap between the modular organization of structural and functional brain networks. *Neuroimage* **257**, 119323 (2022). https://doi.org:10.1016/j.neuroimage.2022.119323

52 Gu, S. *et al.* Optimal trajectories of brain state transitions. *Neuroimage* **148**, 305-317 (2017). https://doi.org:10.1016/j.neuroimage.2017.01.003

53 Betzel, R. F., Gu, S., Medaglia, J. D., Pasqualetti, F. & Bassett, D. S. Optimally controlling the human connectome: the role of network topology. *Sci Rep* **6**, 30770 (2016). https://doi.org:10.1038/srep30770

54 Stiso, J. *et al.* White Matter Network Architecture Guides Direct Electrical Stimulation through Optimal State Transitions. *Cell Rep* **28**, 2554-2566 e2557 (2019). https://doi.org:10.1016/j.celrep.2019.08.008

55 Cui, Z. *et al.* Optimization of energy state transition trajectory supports the development of executive function during youth. *eLife* **9** (2020). https://doi.org:10.7554/eLife.53060

56 Wu, Z. *et al.* Graph deep learning for the characterization of tumour microenvironments from spatial protein profiles in tissue specimens. *Nat Biomed Eng* **6**, 1435-1448 (2022). https://doi.org:10.1038/s41551-022-00951-w

57 Gao, Z. *et al.* Hierarchical graph learning for protein-protein interaction. *Nat Commun* **14**, 1093 (2023). https://doi.org:10.1038/s41467-023-36736-1

58 Burt, J. B. *et al.* Hierarchy of transcriptomic specialization across human cortex captured by structural neuroimaging topography. *Nat Neurosci* **21**, 1251-1259 (2018). https://doi.org:10.1038/s41593-018-0195-0

59 Margulies, D. S. *et al.* Situating the default-mode network along a principal gradient of macroscale cortical organization. *Proc Natl Acad Sci U S A* **113**, 12574-12579 (2016). https://doi.org:10.1073/pnas.1608282113

60 Huntenburg, J. M., Bazin, P. L. & Margulies, D. S. Large-Scale Gradients in Human Cortical Organization. *Trends Cogn Sci* **22**, 21-31 (2018). https://doi.org:10.1016/j.tics.2017.11.002

61 Murray, J. D. *et al.* A hierarchy of intrinsic timescales across primate cortex. *Nat Neurosci* **17**, 1661-1663 (2014). https://doi.org:10.1038/nn.3862

62 Raut, R. V., Snyder, A. Z. & Raichle, M. E. Hierarchical dynamics as a macroscopic organizing principle of the human brain. *Proc Natl Acad Sci U S A* **117**, 20890-20897 (2020). https://doi.org:10.1073/pnas.2003383117

63 Hill, J. *et al.* Similar patterns of cortical expansion during human development and evolution. *Proc Natl Acad Sci U S A* **107**, 13135-13140 (2010). https://doi.org:10.1073/pnas.1001229107

64 Felleman, D. J. & Van Essen, D. C. Distributed hierarchical processing in the primate cerebral cortex. *Cereb Cortex* **1**, 1-47 (1991). https://doi.org:10.1093/cercor/1.1.1-a

65 Goldman-Rakic, P. S. Topography of cognition: parallel distributed networks in primate association cortex. *Annu Rev Neurosci* **11**, 137-156 (1988). https://doi.org:10.1146/annurev.ne.11.030188.001033

66 Sydnor, V. J. *et al.* Cortical-subcortical structural connections support transcranial magnetic stimulation engagement of the amygdala. *Sci Adv* **8**, eabn5803 (2022). https://doi.org:10.1126/sciadv.abn5803

67 Hyde, J. *et al.* Efficacy of neurostimulation across mental disorders: systematic review and meta-analysis of 208 randomized controlled trials. *Mol Psychiatry* **27**, 2709-2719 (2022). https://doi.org:10.1038/s41380-022-01524-8

68 Klooster, D. C. W., Ferguson, M. A., Boon, P. & Baeken, C. Personalizing Repetitive Transcranial Magnetic Stimulation Parameters for Depression Treatment Using Multimodal Neuroimaging. *Biol Psychiatry Cogn Neurosci Neuroimaging* **7**, 536-545 (2022). https://doi.org:10.1016/j.bpsc.2021.11.004

69 Glasser, M. F. *et al.* The Minimal Preprocessing Pipelines for the Human Connectome Project. *NeuroImage* **80**, 105-124 (2013). https://doi.org:10.1016/j.neuroimage.2013.04.127

70 Ciric, R. *et al.* Mitigating head motion artifact in functional connectivity MRI. *Nature Protocols* **13**, 2801-2826 (2018). https://doi.org:10.1038/s41596-018-0065-y

71 Ciric, R. *et al.* Benchmarking of participant-level confound regression strategies for the control of motion artifact in studies of functional connectivity. *NeuroImage* **154**, 174-187 (2017). https://doi.org:10.1016/j.neuroimage.2017.03.020

72 Jenkinson, M., Bannister, P., Brady, M. & Smith, S. Improved optimization for the robust and accurate linear registration and motion correction of brain images. *Neuroimage* **17**, 825-841 (2002).

73 Faskowitz, J., Esfahlani, F. Z., Jo, Y., Sporns, O. & Betzel, R. F. Edge-centric functional network representations of human cerebral cortex reveal overlapping system-level architecture. *Nature Neuroscience* **23**, 1644-1654 (2020). https://doi.org:10.1038/s41593-020-00719-y

74 Cieslak, M. *et al.* QSIPrep: an integrative platform for preprocessing and reconstructing diffusion MRI data. *Nature Methods* **18**, 775-778 (2021). https://doi.org:10.1038/s41592-021-01185-5

75 Tournier, J.-D. *et al.* MRtrix3: A fast, flexible and open software framework for medical image processing and visualisation. *NeuroImage* **202**, 116137 (2019). https://doi.org:10.1016/j.neuroimage.2019.116137

76 Veraart, J. *et al.* Denoising of diffusion MRI using random matrix theory. *NeuroImage* **142**, 394-406 (2016). https://doi.org:10.1016/j.neuroimage.2016.08.016

77 Kellner, E., Dhital, B., Kiselev, V. G. & Reisert, M. Gibbs-ringing artifact removal based on local subvoxel-shifts. *Magnetic Resonance in Medicine* **76**, 1574-1581 (2016). https://doi.org:10.1002/mrm.26054

78 Tustison, N. J. *et al.* N4ITK: Improved N3 Bias Correction. *IEEE Transactions on Medical Imaging* **29**, 1310-1320 (2010). https://doi.org:10.1109/TMI.2010.2046908

79 Andersson, J. L. R., Graham, M. S., Zsoldos, E. & Sotiropoulos, S. N. Incorporating outlier detection and replacement into a non-parametric framework for movement and distortion correction of diffusion MR images. *NeuroImage* **141**, 556-572 (2016). https://doi.org:10.1016/j.neuroimage.2016.06.058

80 Hagmann, P. *et al.* Mapping the Structural Core of Human Cerebral Cortex. *PLOS Biology* **6**, e159 (2008). https://doi.org:10.1371/journal.pbio.0060159

81 Roberts, J. A., Perry, A., Roberts, G., Mitchell, P. B. & Breakspear, M. Consistency-based thresholding of the human connectome. *NeuroImage* **145**, 118-129 (2017). https://doi.org:10.1016/j.neuroimage.2016.09.053

82 Ge, J. *et al.* Increasing diversity in connectomics with the Chinese Human Connectome Project. *Nat Neurosci* **26**, 163-172 (2023). https://doi.org:10.1038/s41593-022-01215-1

83 You, J., Ying, R. & Leskovec, J. Design Space for Graph Neural Networks. (2021). https://doi.org:10.48550/arXiv.2011.08843

84 Kingma, D. P. & Ba, J. Adam: A Method for Stochastic Optimization. (2017). https://doi.org:10.48550/arXiv.1412.6980

85 Maslov, S. & Sneppen, K. Specificity and Stability in Topology of Protein Networks. *Science* **296**, 910-913 (2002). https://doi.org:10.1126/science.1065103

86 Rubinov, M. & Sporns, O. Complex network measures of brain connectivity: Uses and interpretations. *NeuroImage* **52**, 1059-1069 (2010). https://doi.org:10.1016/j.neuroimage.2009.10.003